

Article

Mapping Windthrow Severity as Change in Canopy Cover in a Temperate Eucalypt Forest

Nina Hinko-Najera ^{1,*}, Paul D. Bentley ¹, Samuel Hislop ², Alison C. Bennett ^{3,4}, Jamie E. Burton ¹, Thomas A. Fairman ⁵, Sacha Jellinek ^{3,6}, Julio C. Najera Umana ¹ and Lauren T. Bennett ¹

¹ School of Agriculture, Food and Ecosystem Sciences, Faculty of Science, The University of Melbourne, Creswick, VIC 3363, Australia; paul.bentley@unimelb.edu.au (P.D.B.); jamie.burton@unimelb.edu.au (J.E.B.); julio.najeraumana@unimelb.edu.au (J.C.N.U.); ltb@unimelb.edu.au (L.T.B.)

² School of Science, Geospatial Science, RMIT University, Melbourne, VIC 3000, Australia; samuel.hislop@rmit.edu.au

³ School of Agriculture, Food and Ecosystem Sciences, Faculty of Science, The University of Melbourne, Richmond, VIC 3121, Australia; alison.bennett@csiro.au (A.C.B.); sachamj@unimelb.edu.au (S.J.)

⁴ Commonwealth Scientific and Industrial Research Organisation (CSIRO), Aspendale, VIC 3195, Australia

⁵ School of Agriculture, Food and Ecosystem Sciences, Faculty of Science, The University of Melbourne, Parkville, VIC 3010, Australia; thomas.fairman@unimelb.edu.au

⁶ Waterways, Biodiversity & Environment, Melbourne Water, Docklands, VIC 3008, Australia

* Correspondence: n.hinkonajera@unimelb.edu.au

Abstract: Storm events are significant disturbance agents that can cause considerable forest damage through windthrow. Assessment and mapping of the extent and severity of windthrow is critical to provide reliable information to forest managers to prioritize post-storm hazard reduction (including public safety and fire risk) and to guide restoration activities. Detailed on-ground assessments after windthrow are often impossible due to lack of access and safety concerns. In 2021, severe windstorms caused unprecedented and extensive windthrow in a temperate eucalypt forest in south-eastern Australia. The purpose of this study is to quantify the severity and extent of the damaged forest area as the change in percentage canopy cover using remotely sensed data. We assessed percentage canopy cover from high-resolution aerial images of 455 randomly selected plots in disturbed and undisturbed areas to train a model and machine learning framework to predict landscape scale canopy cover from Sentinel-2 images. A random forest model using all single bands and percentiles best predicted the canopy cover ($R^2 = 0.69$). Sentinel-2 images were then used to predict canopy cover pre- and post-windthrow to assess and map the severity of windthrow as the change in percentage canopy cover. Of the total 63,471 ha of forest area assessed, 63% (39,987 ha) was impacted by windthrow, with 46% at low severity (<30% canopy cover loss), 11% at moderate (30–50% canopy cover loss) and 6% at high severity (>50% canopy cover loss). Our study provides the first quantitative mapping of windthrow severity mapping for a temperate eucalypt forest in Australia that demonstrates an effective remote assessment methodology and provides critical information to support post-windthrow management decisions.

Keywords: Sentinel-2; Nearmap Australia; temperate broadleaved evergreen forest; Wombat Forest; change detection; tidymodels; random forest; windstorm; forest disturbance; Australia



Citation: Hinko-Najera, N.; Bentley, P.D.; Hislop, S.; Bennett, A.C.; Burton, J.E.; Fairman, T.A.; Jellinek, S.; Najera Umana, J.C.; Bennett, L.T. Mapping Windthrow Severity as Change in Canopy Cover in a Temperate Eucalypt Forest. *Remote Sens.* **2024**, *16*, 4710. <https://doi.org/10.3390/rs16244710>

Academic Editors: Jian Yang and Lei Fang

Received: 21 October 2024

Revised: 12 December 2024

Accepted: 13 December 2024

Published: 17 December 2024



Copyright: © 2024 by the authors. Licensee MDPI, Basel, Switzerland. This article is an open access article distributed under the terms and conditions of the Creative Commons Attribution (CC BY) license (<https://creativecommons.org/licenses/by/4.0/>).

1. Introduction

Severe storm events are significant natural disturbance agents that can cause considerable forest damage through windthrow, i.e., the uprooting and stem breakage of trees. Extensive windthrow can cause immediate changes to the structure, composition, and function of forest ecosystems. These events can further impact forest dynamics and diverse processes from the stand to landscape scales, including forest growth, successional trajectories, carbon sequestration, evapotranspiration and water yield, biodiversity, fuel

accumulation, and fire behaviour [1–4]. Windthrow has additional impacts on the socio-economic values of forests including risks to public safety posed by post-storm tree fall and through loss of timber, amenity values and recreational areas [5]. Climate change is increasing the frequency, intensity, and extent of weather extremes and, thus, wind-related disturbance regimes [6–10] with severe storms predicted to increase in previously unaffected regions [11]. However, considerable uncertainty remains about post-windthrow forest dynamics will respond [12,13].

The occurrence and severity of windthrow primarily depends on the intensity and duration of the storm event. In mid-latitude temperate zones of both the northern and southern hemisphere, such extreme storm events are commonly attributed to extra-tropical cyclones, large-scale systems that produce wind speeds up to 120 km/h and which are often accompanied or preceded by high rainfall [3]. In temperate (southern) Australia, however, severe thunderstorms are often the major source of severe convective winds defined by gusts exceeding 90 km/h and associated with extreme rainfall, hail storms, and/or tornadoes [14,15]. Wind damage to trees can include complete or partial uprooting, tree lean, and stem breakage, and depends on individual tree characteristics (root architecture, height/diameter ratio), stand structures (multi-or even aged), and site conditions (topography, soil properties, and soil water) [11,16–18]. Consequently, characterization of wind damage severity is often based on the quantity or proportion of fallen stems within an area, canopy damage, change in canopy cover, and tree mortality (e.g., [2,3,11,16,19]). The extent of windthrow can range from small-scale localized damage of a few or single trees to landscape-scale damage across hundreds of hectares [3].

The assessment and mapping of the extent and severity of windthrow is critical to better understand patterns of damage to forests and to provide reliable information for post-storm management decisions. However, existing methods, such as field surveys, are laborious, time-consuming and limited by restricted access and hazards posed by fallen and leaning trees, making comprehensive landscape-scale assessments impossible. Recent and advancing methods that use ground-based, airborne, and satellite remote sensing products allow for more efficient, cost-effective landscape-scale assessments of forest damage at high spatial resolution and accuracy as well as monitoring over time [11,20,21]. Remote sensing products to map and assess windthrown areas range from high-resolution aerial imagery using unmanned aerial vehicles (UAVs), airplanes, or satellites [19,22,23] or airborne laser scanner data (ALS) [24,25] to Sentinel-1 synthetic aperture radar (S1) data [26–29], and multispectral optical satellite imagery data at medium (Landsat) and high (Sentinel-2, S2) spatial resolution [30–35]. Each product has advantages and limitations, with considerable variation in spatial and temporal resolution, availability, and costs. Airborne imagery or ALS can provide very high-resolution outputs and can detect small-scale (i.e., single tree) changes, but typically have high acquisition costs, limiting data availability and coverage at broad scales [19,23,25]. Many recent studies have emphasized the potential of S2 data to detect windthrow with freely available online multispectral (13 bands) optical satellite images that have global coverage at high spatial resolution (10 m) and high revisit frequency (5 days) [29,33].

Few methods for mapping windthrow areas with remote sensing data provide information about the severity of windthrow beyond a binary classification (damaged and undamaged) [29,33,36,37]. Since trees define a forest, the severity of forest windthrow can be defined and quantified in terms of the degree of loss of tree canopy cover. So far there are few methods available that quantitatively assess windthrow severity in forests on a continuous scale across large areas [24,38,39]. Most mapping methods are focused on fast detection, delineation, and process automatization using advanced machine-learning methods [31,32,37]. Such methods are frequently based on change detection that use vegetation indices as proxies for forest status and function, derived from either post-disturbance-only imagery or pre- and post-disturbance imagery including a range of different times since the disturbance event [29,30,33,34,40]. However, there remains considerable scope to simplify these methods to improve transferability across forest types and biomes, including

examining the utility of single bands to indicate windthrow-severity (as opposed to indices that are calculated from those bands [29]).

Windthrow in temperate forests in south-eastern Australia has been typically limited to small areas, although occurrences of (damaging) windstorms are not uncommon [41]. There are few examples of windthrow impacts and damage to temperate forests, and these have only been reported in isolated and localized cases in broadleaved evergreen eucalypt forests [42–44] or pine plantations [45]. Otherwise, most studies have focused on windthrow associated with cyclones of the wet tropics of northern and north-eastern Australia [39,46]. In June 2021, a major storm caused extensive areas of windthrow throughout temperate eucalypt forests in Central Victoria in south-eastern Australia, providing a unique opportunity to develop specific windthrow severity methods for temperate native forests of complex structure.

A better understanding of windthrow severity patterns will help with managing forest recovery efforts, including for public safety, as well as potential interactions with other landscape-scale disturbances, like wildfire [47]. While effective and well-established methods for fire-severity classification and mapping from multispectral optical satellite data exist for the fire-prone landscapes of south-eastern Australia [48–50], they are not suited to areas affected by windthrow. Fire-severity mapping is based on a decrease in greenness, whereas windthrow changes the distribution of greenness through loss of the tree canopy cover and the persistence of greenness in the understory. Fire and windthrow can also differ in their impacts on forest structure and vegetation damage; for example, burnt trees often remain standing, while forests affected by windthrow result in large amounts of woody debris being deposited on the ground. Differences in greenness between windthrow and fire damage can also occur post-disturbance with distinct spatial and temporal patterns of overstory and understory recovery, i.e., resprouting of damaged tree stems might occur faster after fire than windthrow. Therefore, fire-severity classification methods might underestimate the true severity of windthrow, necessitating the development of a separate method to safely and accurately assess windthrow severity from stand to landscape scales.

In this study, we assess and quantify the extent and severity of an extensive windthrow event in a eucalypt forest landscape of temperate south-eastern Australia. We develop and test a novel change-detection approach that combines very high-resolution aerial images with high-resolution multispectral satellite (S2) data. Using this approach, we spatially predict the extent and severity of windthrow based on the change in percentage canopy cover.

Our objectives are as follows:

- To test regression models based on high-resolution remote sensing data for estimating forest canopy cover before and after windthrow in broadleaf evergreen eucalypt-dominated forests.
- To use the best performing model to assess and quantify windthrow severity based on percentage change in forest canopy cover.
- To provide a continuous map of windthrow severity across the study landscape.

Overall, we aim to improve the availability of practicable methods for quantifying windthrow severity—from isolated patches to complex landscapes—in native eucalypt forests of temperate Australia and thereby provide a stronger basis to support decisions in the aftermath of windthrow events.

2. Materials and Methods

2.1. Study Area

The study area is located within an extensive temperate forest area in south-eastern Australia (known as the Wombat State Forest, hereafter ‘Wombat Forest’) about 100 km north-west of Melbourne, Victoria. The forest is about 70,000 ha in area and spans across Victoria’s Great Dividing Range with elevations from 590 to 760 m above sea level and an underlying geology of Ordovician marine sedimentary rocks. Soils are moderate to highly weathered and classified as kandosols (“stony earths”) and dermosols, acidic-mottled

duplex soils [51]. The climate is cool temperate, with wet cold winters and dry warm to hot summers. The long term mean annual rainfall is 880 mm, predominantly falling in winter and spring [52]. Mean monthly maximum temperatures range from 7 °C (July) to 24 °C (January), with daily summer temperatures often exceeding 35 °C, while frosts are common in winter [53] and mean monthly minimum temperatures range from 2 °C in winter to 12 °C in summer [54,55].

The temperate evergreen eucalypt forest is classified as an open forest with tree heights ranging from 10 to >30 m, a projective foliage cover from 30 to 70% [56], and basal areas of 30–45 m² ha⁻¹ [54,55]. Open- to tall-open forests are widely distributed across Victoria and are moderately productive, thus storing the majority of Victoria's forest carbon [54,55,57]. The Wombat State Forest is dominated by a mix of fire-tolerant eucalypts (i.e., mature trees capable of resprouting and surviving fire), typically *Eucalyptus obliqua* L'Hér., *Eucalyptus radiata* Sieber ex DC., and *Eucalyptus rubida* H. Deane and Maiden. The understorey consists of a sparse shrub layer of 2–4 m height, and a discontinuous ground layer dominated by Austral bracken (*Pteridium esculentum* (G. Forst) Cockayne) with native perennial grasses, forbs, and rushes [58].

The Wombat Forest encompasses the lands of the Wurundjeri Woi Wurrung, Wadawurrung, and Dja Dja Wurrung peoples [59]. Post-colonization forest history included timber harvesting, beginning with extensive clearing during the Goldfields era (1850s to early 1900s), and then for the operation of local saw mills through selective harvesting until early 1970, followed by more intensive shelterwood systems until the 2000s [60]. From 2003 to 2005, the Wombat Forest was part of a community forest management trial [61]. Timber harvesting was then significantly reduced and ceased by mid-2024 with only local firewood collection in designated areas remaining. These forest types are prone to occasional wildfire, with the last known wildfire in 2009, and, thus, general forest management includes low-intensity prescribed fires to reduce fuel hazard, a common practice across public land in Victoria since the 1960s [53,55].

2.2. Storm Event and Methodology Workflow

On the 9 June 2021, parts of Victoria, Australia, were impacted by a severe storm event accompanied and preceded by heavy rainfall due to severe convective winds (likely with small tornadoes) at higher elevations with prolonged high wind speeds and gusts up to 130 km/h [15]. It is noted that the reported wind speeds are from Melbourne Airport, about 70–120 km west of the forest area and at a lower elevation (132 m). The release of strong convection was associated with orographic uplifting, so that the destructive wind gusts occurred in higher-elevation areas of Central Victoria [15]. This event caused windthrow that was unprecedented in extent and severity across Central Victoria in south-eastern Australia. A subsequent windstorm on the 29th of October 2021 caused further but relatively minor damage in already affected forest areas compared to the June storm (Figure 1).

To assess the extent and severity of windthrow, we used regression models to predict canopy cover across the Wombat Forest area both before and after the windthrow event. We used plot-scale estimates of percentage canopy cover derived from visual assessments of very high-resolution aerial images of plots, selected using stratified random sampling. Ground-truthing of canopy cover estimates was not possible due to the access restrictions posed by the forest management agency and high safety risks from fallen and leaning trees and loose branches.



Figure 1. An example of severe windthrow in the Wombat Forest from high-resolution aerial images [62]: (a) pre-disturbance in December 2020 and (b) post-disturbance in December 2021, and (c) on-ground photo shortly after windthrow and first response in road access clearance (June 2021).

Cover estimates were used to develop and train a regression model using single bands and selected vegetation indices from S2 images as predictor/input variables. The pre- to post-windthrow difference in percentage canopy cover was then used to determine windthrow severity across the forest area (see Figure 2 for a summary of the method workflow).

Data mining, processing, modelling (machine learning), and analysis were undertaken using the R programming language [63], including the packages ‘slippymath’ [64], ‘sf’ [65,66], and ‘terra’ [67].

2.3. Plot Selection

The stratified random sampling of assessment plots was guided using the difference in the Normalized Burn Ratio (dNBR) to initially distinguish between undamaged and damaged forest areas. The indicative map based on a dNBR threshold of >0.15 was derived from S2 images collected pre-storm (December 2020) and post-storm (December 2021) and processed using Google Earth Engine (GEE) [68]. The selected time period aligned with the regular annual collection of very-high-resolution images [62] across the forest, which were later used to remotely assess canopy cover for each plot. From the indicative map, small clumps of pixels (<9) were removed, and to capture areas adjacent to damaged areas, as suggested by [69] a 20 m buffer (2 pixel) was created around the damaged areas. A total of 200 plots (3×3 pixel = 30×30 m = 0.09 ha) were randomly selected within the damaged areas, with a further 50 plots within the buffer area and 100 plots in the undamaged area. These 350 plots were later used to assess post-storm canopy cover from Nearmap images from 2021. An additional 105 plots (60 within the damaged area in 2021, 15 from the buffer area in 2021, and 30 from the undamaged area) were randomly selected for later assessment

of pre-storm canopy cover from Nearmap images from 2020. This resulted in a total number of 455 plots (Figure 3), equivalent to 0.1% of the Wombat Forest's area.

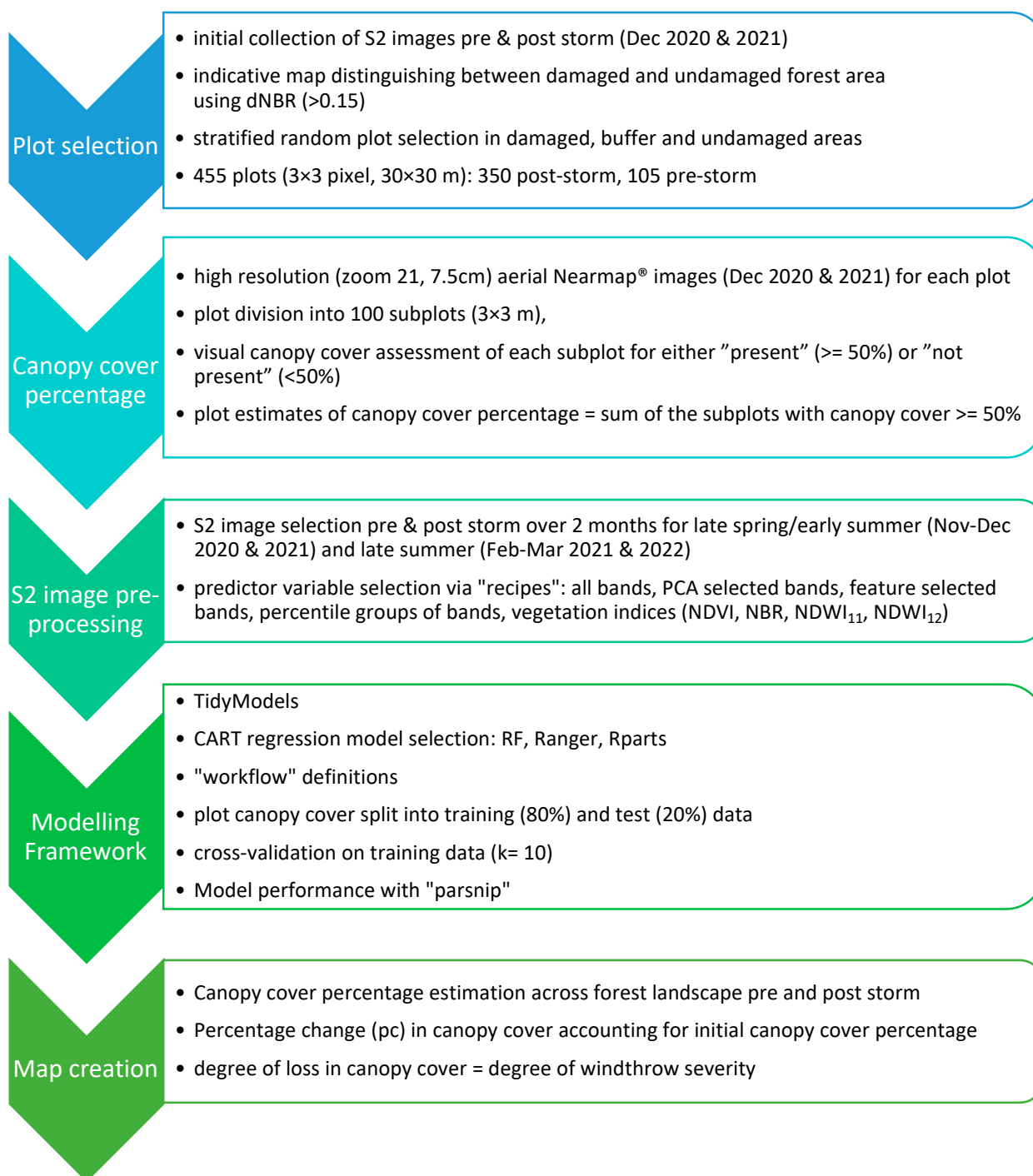


Figure 2. Workflow of methodology; S2: Sentinel-2, dNBR: difference in the Normalized Burn Ratio; PCA: principal component analysis selection; feature selection includes the potential removal of variables with large absolute correlations with other variables, and normalizing variables to have a mean of zero and a standard deviation of one. Percentile groups: 10th, 25th, 50th, 75th, and 95th.

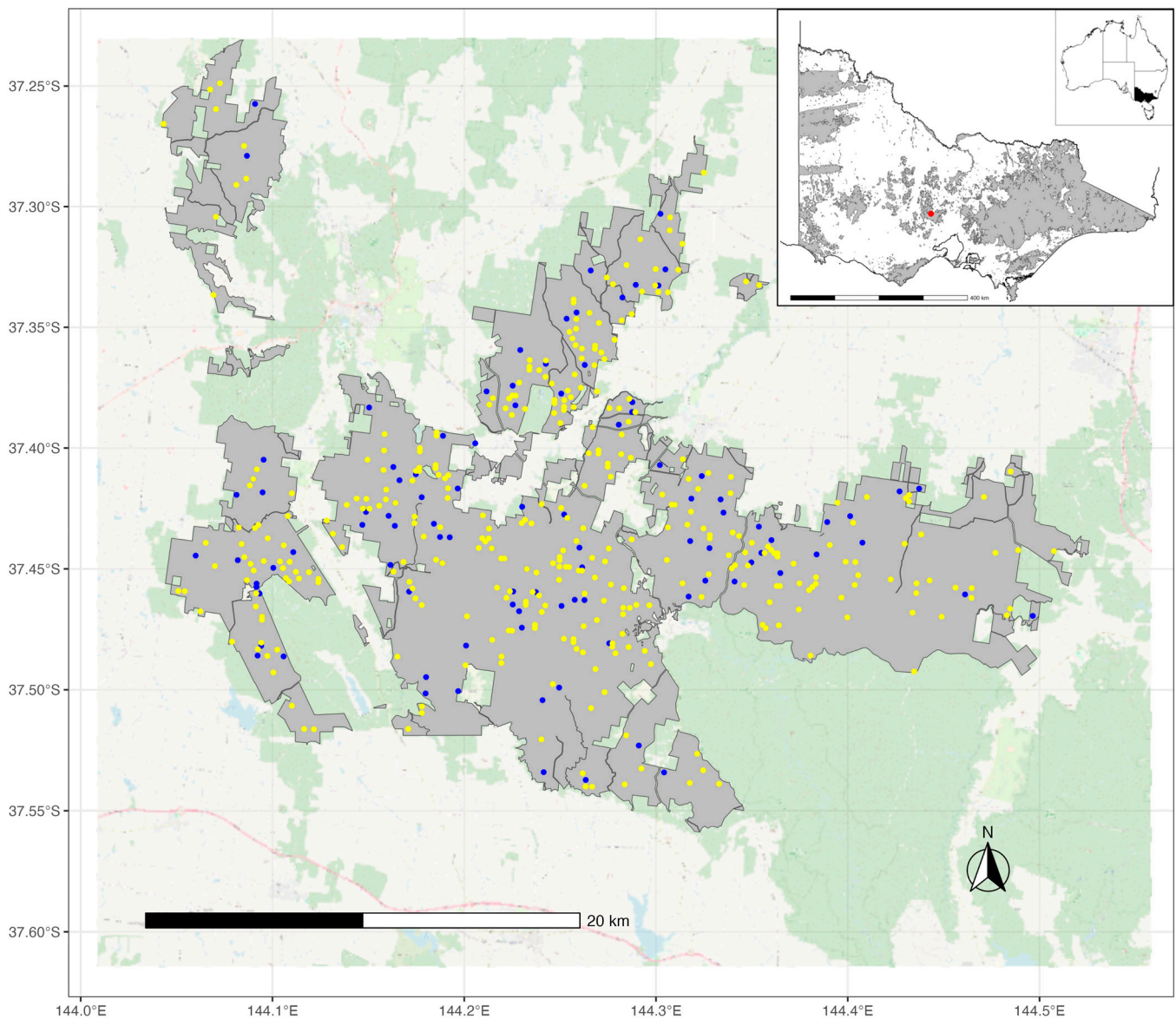


Figure 3. Location of the study area, namely the Wombat State Forest (grey) in Central Victoria (red dot in Victoria inset map), in south-eastern Australia. Points on the main map indicate sampling plots (30 × 30 m) post-windthrow (yellow) and pre-windthrow (blue), evenly distributed between damaged and non-damaged areas based on the initial dNBR threshold (>0.15).

2.4. Canopy Cover Percentage Assessment

For each plot, high-resolution aerial images [62] were extracted using a 30 m buffer around each plot center point at the maximum resolution available (zoom 21, 7.5 cm). Each plot image was visually assessed for canopy cover percentage by dividing the plot image into 100 3 × 3 m subplots, and then each subplot was manually assessed for canopy cover of either “present” (≥50%) or “not present” (<50%), with the total sum of “present” subplots being the total percentage canopy cover per plot (Figure 4). Images were available from 14 December 2020 as the pre-storm condition (six months before the event) and from 20 December 2021 as the post-storm condition (six months after the event) [62]. The assessment of the total of 455 plot images was divided among the 9 co-authors to ensure objectivity. Each co-author visually assessed 56 plot images following a detailed protocol to assure quality and consistency. This included a 10% overlap of each co-author’s set of plots, i.e., 6 images per assessor or 54 in total were assessed twice, to ensure that the visual analysis was reproducible and evaluated to minimize the subjective error.

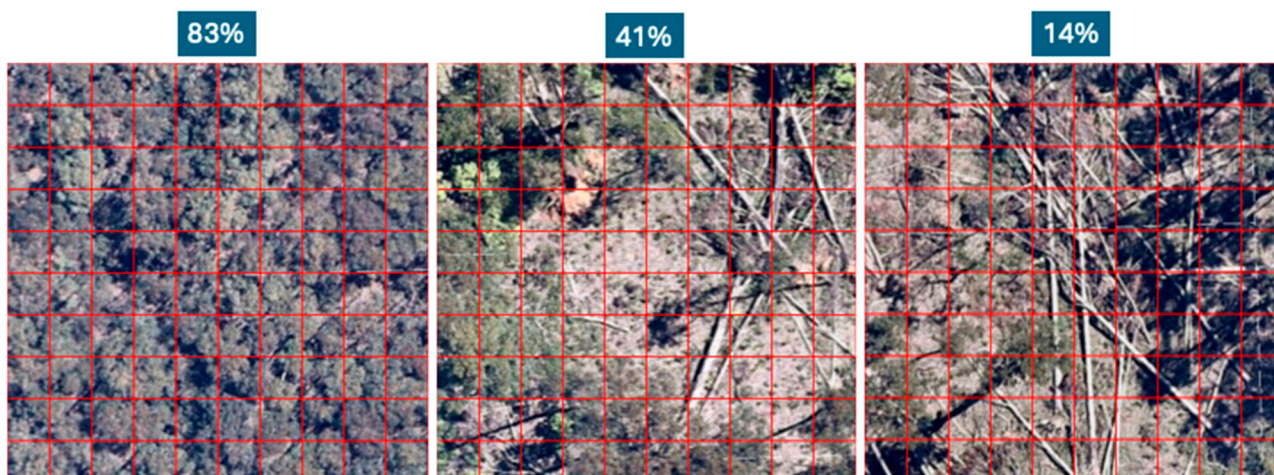


Figure 4. Example to illustrate the percentage canopy cover assessment of high-resolution aerial images from December 2021 (post-windthrow, Nearmap Australia, 2022) of three different 30×30 m plots. Each plot is split into 3×3 m subplots used to record either the presence ($\geq 50\%$) or absence ($< 50\%$) of canopy cover; values above the pictures are the total percentage canopy cover of the plot calculated as the ratio of subplots with canopy present divided by the total number of subplots.

2.5. S2 Image Preprocessing and Feature Engineering

Sentinel-2 is a wide-swath, high-resolution, multispectral imaging mission supporting Copernicus Land Monitoring studies, including the monitoring of vegetation, soil, and water cover. This study utilized Sentinel-2 Harmonized Level-2A imagery [70], which provides bottom-of-atmosphere (BOA) reflectance values corrected for atmospheric effects using the Sen2Cor tool version 2.11.0 [71] developed by the European Space Agency [72]. The harmonized dataset ensures consistency in spectral and temporal data. Cloud masking was applied using two approaches: first, the Sentinel-2 cloud probability data, which filters out pixels with high cloud probability to enhance data quality (maximum cloud probability = 10%) was used; and second, the scene classification layer (SCL) method was used, which further refines the dataset by masking clouds and isolating vegetative cover for targeted analysis. The selection of Sentinel-2 data was influenced by its inbuilt functionality and seamless integration with GEE [68], which provides access to harmonized datasets, cloud probability layers, and SCL bands, simplifying processing and enabling efficient analysis. This combination of masking techniques and platform capabilities ensures accurate surface reflectance values, supporting the reliable detection of storm impacts and post-storm environmental changes, as well as the reproducibility of workflows using open access platforms. GEE [68] was used to generate a data cube of S2-derived single bands and indices as predictors for the landscape-scale regression model (Table 1). S2 imagery was extracted from two 2-month periods: early summer (November and December), to overlap with the available time period of high-resolution aerial imagery [62] that was used for our plot-level estimation of percentage canopy cover; and late summer (February and March), to allow for a stronger contrast in spectral signals between the canopy of remaining trees (overstory) and dried-out shallow rooted and annual understory vegetation (e.g., grass, bracken) as well as canopy browning (die-off) of fallen trees.

Table 1. Predictor variable grouping and recipe definition.

Period	Predictor Variable	Selection	Recipe
Nov–Dec	single bands	all	all feature-selected PCA
		percentile ranges	all feature-selected PCA
	indices	all individual	- -
Feb–Mar	single bands	all	all Feature-selected PCA
		percentile ranges	all feature-selected PCA
	indices	all individual	- -

Only bands at the 10 to 20 m spatial resolution were used (10 bands in total), with resampling to 10 m of the 20 m bands with a nearest neighbor approach. A 3×3 S2-pixel focal smoothing window (30×30 m) was applied using [67] to calculate the mean value of all cells within the window, with the resulting value assigned to the central 10×10 m pixel. The S2 collection was processed to generate a mosaic image for the percentiles (10th, 25th, 50th, 75th, and 95th) across all bands for each grid cell and to estimate the following indices: NDVI, NBR, NDWI₁₁, and NDWI₁₂. All chosen vegetation indices have been previously used in different disturbance assessments, e.g., windthrow [29,33,40,73] or fire severity [48–50], and are based on their bands' sensitivity to variations in chlorophyll content and biomass (NIR, RED) and water content (SWIR), and they have been shown to be effective in the detection of storm damages [40,73,74]. Aggregating time-series satellite data into temporal–spectral percentiles is a common technique [75] to address gaps caused by cloud cover while preserving differences in phenological characteristics and water use over the time period.

The NDVI (Normalized Difference Vegetation Index) was calculated as the ratio of the NIR (S2-Band 8) and RED (S2-Band 4), as follows:

$$\text{NDVI} = (\text{NIR} - \text{RED}) / (\text{NIR} + \text{RED}) \quad (1)$$

The NBR (Normalized Burn Ratio) was calculated as the ratio of the NIR (S2-Band 8) and SWIR (S2-Band 12), as follows:

$$\text{NBR} = (\text{NIR} - \text{SWIR}) / (\text{NIR} + \text{SWIR}). \quad (2)$$

The NDWI (Normalized Difference Water Index) was calculated as the ratio of the narrow NIR (S2-Band 8A) and SWIR (S2-Band 11 or S2-Band 12) [76], as follows:

$$\text{NDWI}_{11 \text{ or } 12} = (\text{nNIR} - \text{SWIR}_{11 \text{ or } 12}) / (\text{nNIR} + \text{SWIR}_{11 \text{ or } 12}) \quad (3)$$

Feature engineering and data preprocessing—consisting of the creation, transformation, extraction, and selection of predictor variables that were most conducive to creating an accurate machine learning algorithm—were undertaken using the “TidyModels” framework [77]. Predictor variable recipe definition (Table 1) included the following:

- All single bands with three different recipes: (1) all single bands, (2) principal component analysis (PCA)-selected bands, and (3) feature-selected bands (potential removal

of variables with strong absolute correlations with other variables, and normalized variables to have a mean of zero and a standard deviation of one).

- Percentiles (10th, 25th, 50th, 75th, and 95th) of single bands from their distribution across the selected 2-month periods with three different recipes: all available single bands, PCA-selected bands, and feature-selected bands.
- The above-mentioned selected indices.

2.6. Modelling Framework

2.6.1. Model Selection

CART (classification and regression tree) models were selected as they generally provide robust results for ecological applications using remote sensing data due to their ability to identify non-linear relationships between the data and threshold and voting systems. The following three regression models were compared:

- Random Forest [78,79], which implements Breiman’s random forest algorithm (based on Breiman and Cutler’s original Fortran code) for classification and regression.
- Ranger [80], a fast implementation of random forests [78] or recursive partitioning, particularly suited for high dimensional data. Regression forests are implemented as in the original random forest [78].
- Rparts [81], a decision-tree model via CART that implements recursive partitioning for classification, regression, and survival trees. An implementation of most of the functionality of [82].

2.6.2. Workflow

The workflow defined a model that creates many decision trees ($n = 1000$), each independent of the others, and using cross-validation sampling ($n = 10$). The final prediction used all predictions from the individual trees and combined them. Optimization was performed using the grid search methods outlined by [77], using tuning parameters for the number of splits at each branch (min_n), the number of predictors that will be randomly sampled at each split when creating the tree models (mtry), and tree depth (maxdepth). The response variable (percentage canopy cover by plot) was split into training (80%) and independent test (20%) data subsets, with the independent test data subset reserved until the end of the project and used as an unbiased source for validation (measuring final model performance) and visualization. A 10-fold cross-validation was applied only on the training data subset to evaluate model performance, and hyperparameters were optimized using a grid search approach, according to [83].

Models were built and compared using the “parsnip” package [84] which is part of the tidymodels framework [77]. This framework simplifies the comparison of model performance based on model performance metrics including the coefficient of correlation (R^2) and root mean square error (RMSE). The final tree of the best model was then selected based on the highest R^2 and lowest RMSE.

2.7. Map Creation of Canopy Cover Percentage and Windthrow Severity

The final tree was used to generate a spatial prediction using the preprocessed S2 image to create rasters of continuous canopy cover pre- and post-windthrow across the wider Wombat Forest area including adjacent areas of the same forest type. The final area of the map was refined to exclude areas of plantations, water bodies, and prescribed burns that occurred in the period between pre-storm image acquisition (Nov 2020) and the storm event (June 2021).

The change in canopy cover and, thus, the indicator for windthrow severity, was calculated as the difference between pre- and post- windthrow canopy cover as a percentage of the pre-storm canopy cover, as follows:

$$PC = (CC_{\text{post}} - CC_{\text{pre}}) / |CC_{\text{pre}}| \times 100 \quad (4)$$

where PC is the percentage change, CC_{post} is the percentage canopy cover post-windthrow, and CC_{pre} is the percentage canopy cover pre-windthrow. Negative values indicate a decrease in canopy cover (i.e., loss through windthrow), while positive values indicate an increase. The more negative the PC, the greater the severity of windthrow.

3. Results

Model Performance

Overall, the random forest (RF) and ranger model engines performed equally well and had better model performance than Rparts. Figure 5 shows the output of the RF model engine for each predictor variable recipe ranked by the highest R^2 (Figure 5a,b) and lowest RMSE (Figure 5c,d) for either time periods Feb–Mar (Figure 5a,c) or Nov–Dec (Figure 5b,d). The overall best performing model included all available single bands across the late summer period (Feb–Mar, $R^2 = 0.68$ (0.02 s), RMSE = 14.6 (0.5 s)). The best performing model for the late spring–early summer period was the model using the 50th percentile of all available single bands ($R^2 = 0.67$ (0.02 s), RMSE = 14.9 (0.5 s)). In comparison, using indices as predictor variables did not improve the model outputs. All selected indices combined had a lower model performance compared to the best single-band model outputs for both periods (Feb–Mar: $R^2 = 0.64$ (0.02 s), RSME = 15.6 (0.5 s); Nov–Dec: $R^2 = 0.62$ (0.03 s), RSME = 15.8 (0.5 s)). The performance of models based on individual indices was even lower than those that used all indices combined or single bands, with different best-performing models based on single indices between periods (NBR in Feb–Mar compared with NDVI in Nov–Dec; Figure 5).

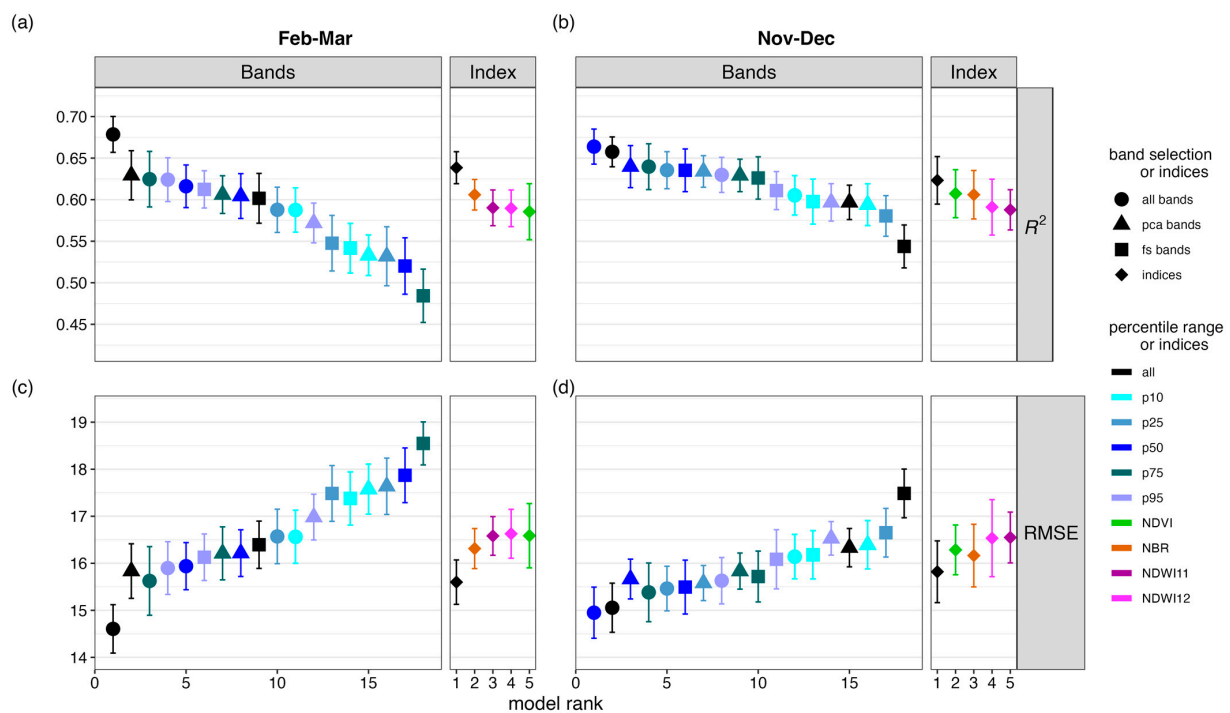


Figure 5. Random-forest model performances for bands (per distribution and combination of bands) and selected indices ranked by highest coefficient of determination (R^2 , upper panels (a,b)) and lowest root mean square error (RMSE, lower panels (c,d)); different shapes represent different indices and combination of selected bands: all single bands used (circles), principal component-selected bands (pca, triangles) and selection of bands accounting for auto-correlation: feature-selected bands (fs, squares, different colors represent different percentile ranges used for bands and individual indices, predictor variables (bands or indices) derived from S2 images in Feb–Mar (mid-late summer, left panels (a,c)) and from Nov–Dec (late spring—early summer, right panels (b,d)).

The final fit of the best RF model with the independent test data set showed a significant correlation between the observed and predicted canopy cover percentage with an adjusted R^2 of 0.69 (Figure 6a) and a negligible pattern in the residuals (Figure 6b). The higher the variable importance, the higher the loss of model accuracy when this variable is excluded. High variable importance indicates an increase in mean square error (i.e., a decrease in accuracy if that variable is excluded from the model). The most important variables in that model were bands 12 and 11 at the highest percentiles (75th, 95th, and 50th) of their distribution (Figure 6c). Bands 12 and 11 from the SWIR (short-wave infrared) region are both indicative for vegetation water content and early water stress detection. The higher percentile metrics allow better spatial-temporal coverage that account for gaps caused by cloud cover while preserving differences in phenological characteristics, water use across heterogenous landscapes and exclude noise due to errors.

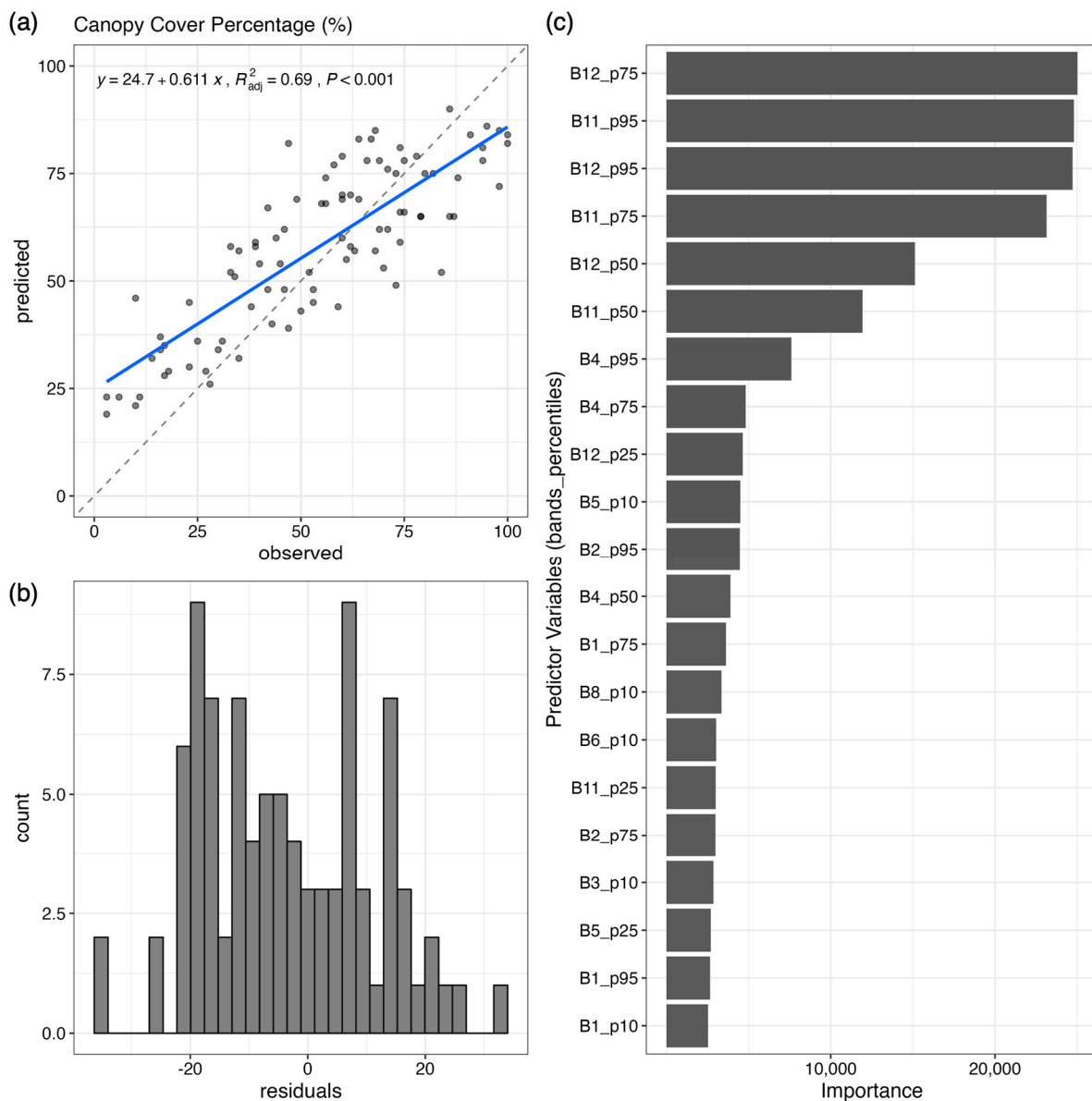


Figure 6. Final fit of the best random-forest model with the independent test data set: (a) correlation between observed and predicted canopy cover percentage; (b) residuals of the fit; (c) predictor variable importances. The most important bands and their percentiles are shown (importance > 2500).

This best RF model was used to predict percentage canopy cover across the study area using S2-images for the pre-windthrow period (Feb–Mar 2021, Figure 7a) and the post-windthrow period (Feb–Mar 2022, Figure 7b). From these maps, the percent change in canopy cover was calculated to estimate the severity of windthrow across the study area based on the change in canopy cover (Figure 7c).

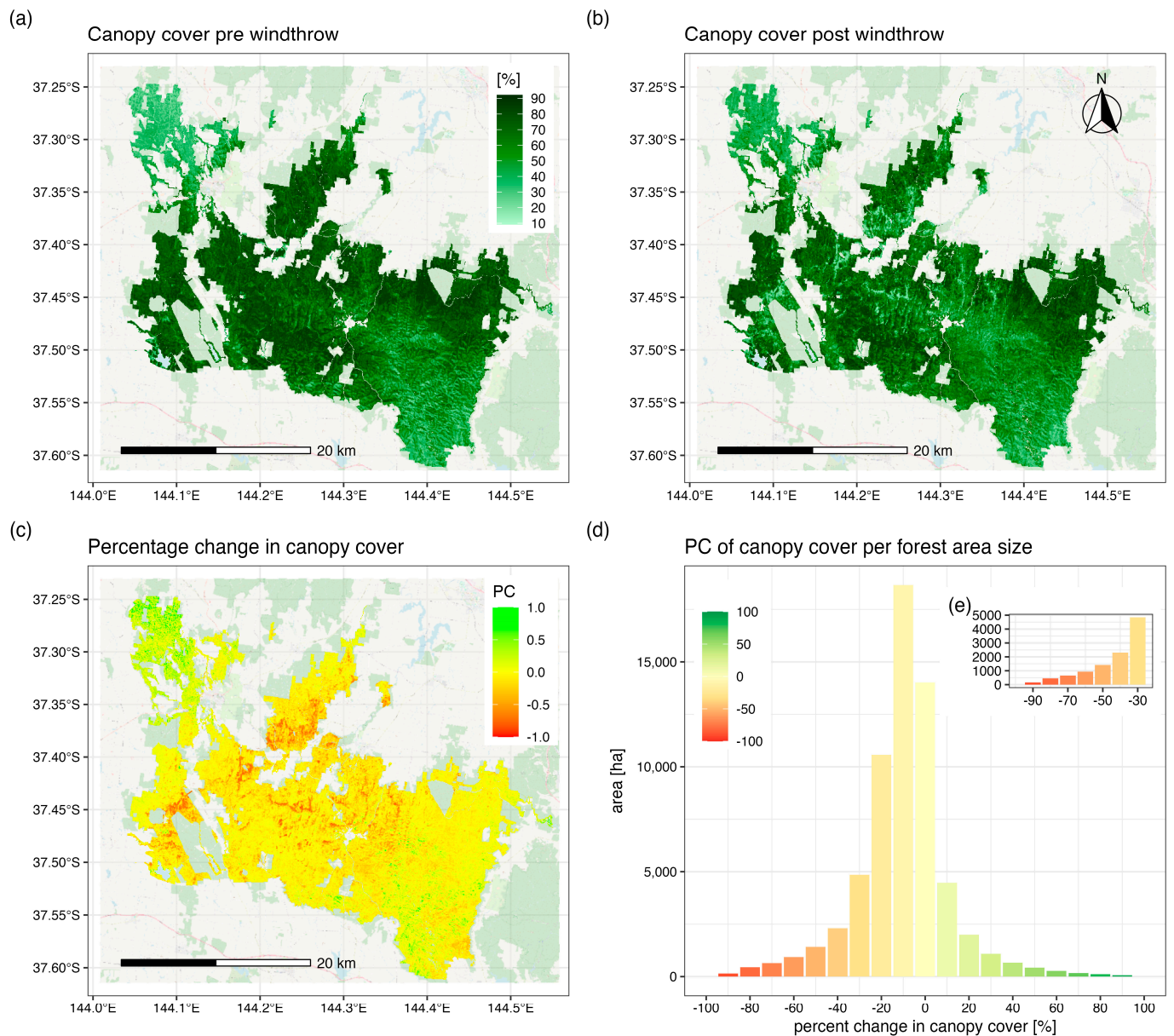


Figure 7. Predicted canopy cover using a random-forest model [%] (a) before (summer 2020/21) and (b) after (summer 2021/22) the windthrow. (c) Percentage change in canopy cover and (d) Percentage change in canopy cover [%] per forest area [ha] across the entire study area. (a,b): the greener the area the higher the canopy cover percentage; (c,d): green and positive values indicate an increase in canopy cover, yellow indicates minimal change, while orange to red and negative values indicate a decrease (loss) in canopy cover through windthrow with increasing severity (from yellow to red); the inset figure (e) provides more detailed information for canopy loss in the -30% to -90% range.

More than half of the forested study area (39,987 ha or 63%) was impacted by windthrow although most of the impacted area (29,233 ha or 46%) was of low severity ($<30\%$ canopy cover loss; Figure 7d, Table 2). A total of 7155 ha (or 11%) of the forested area was affected by

moderate-severity windthrow (canopy cover decrease 30 to 50%), compared with 3599 ha (6%) by high-severity windthrow (>50% canopy cover decrease; Table 2).

Table 2. Study forest area (wider Wombat Forest, and under state forest tenure) and the extent of windthrow as mean change in canopy cover (CC) by low (0 to −30% CC decrease), moderate (−30 to −50%), and high (>−50%) severity.

Forest	Total (ha)		Windthrow (ha)		Low Severity (ha)		Mod Severity (ha)		High Severity (ha)	
Wombat Forest	63,312	100%	39,987	63%	29,233	46%	7155	11%	3599	6%
State Forest	44,101	70%	29,762	67%	21,332	48%	5285	12%	3145	7%

4. Discussion

In this study we demonstrate a methodology for the quantification and mapping of windthrow extent and severity at a high spatial resolution (10 m) across an extensive forested landscape. The method predicts change in percentage canopy cover by combining high-resolution aerial images with multispectral optical satellite data (S2) in a random forest regression modelling framework. To the best of our knowledge, this is the first study to map windthrow severity as a continuous variable across a temperate eucalypt forest in south-eastern Australia.

4.1. Time Period for Change Detection

The best model performance was achieved using S2-images from the late summer period (Feb–Mar) that were 8 to 9 months after the main windthrow event. This could be attributed to the stronger contrast in spectral signals between the remaining intact canopy cover and the, by that time, complete die-off, (browning) of the canopy of fallen trees. The study's forests are dominated by resprouting eucalypts (i.e., trees that can resprout from meristematic tissues in the stem or belowground organs), which is a characteristic feature and adaptation to tolerate and survive defoliation in this fire-prone landscape [85]. However, spectral signals at this time since windthrow were not yet affected by rigorous resprouting from damaged standing or partially standing stems or new seedling growth. Cover of the ground stratum was also at its least in the drier summer months, further contributing to the distinct spectral signal of windthrown areas by late summer. Fairman et al. [47] reported a significant increase in grasses, understory vegetation, and eucalypt seedlings in high windthrow severity areas 2 years after the windthrow event. In a comparable approach to our study, Staben and Evens [39] reported significant windthrow (up to 42% canopy loss) in tropical eucalypt woodlands 10 days after a cyclone, but detected some proportion of canopy recovery one year after the cyclone, likely related to epicormic resprouting of defoliated crowns or along damaged stems [39]. Our time period for post-windthrow assessment agrees well with the reported 8 months required for the most accurate mapping of damaged forest area in the Italian alps using optical remote sensing data [33,34], despite the distinct forest types. Concurrently, studies using change detection methods also highlighted that the least accurate mapping was derived from imagery closer to the disturbance event [33,34,40]. However, forest managers might require a more rapid mapping of windthrow areas immediately after an event to inform emergency responses, including clearing fallen trees and debris from roads and ensuring public safety. For this, an indicative map with potentially lower model performance for windthrow areas might be sufficient, although this was not explicitly tested in this study, as the chosen time period was aligned with the availability of high-resolution aerial images and to encompass additional damage caused by a second storm 4 months after the first. The earliest time period to obtain quality satellite data after a windthrow event might also depend on seasonal weather conditions, since, for example, cloudy conditions are less likely during the summer months in temperate Australia compared to in the winter, when the main storm occurred.

4.2. Limitations

A potential limitation of our methodology compared to other methods is the availability of high-resolution aerial images to remotely assess plot-scale canopy cover, as regular coverage is limited to the most populated areas in Australia [62] and is not freely available. Compared to fully automated rapid-detection methods, our approach involved manual/visual estimation of canopy cover at plot scales; however, automatization of this step is a focus of our ongoing research, including training based on diverse windthrow events across temperate forests in Australia.

4.3. Predictor Variables and Model Performance

The random forest model including all single S2 bands and percentile distributions indicated that the SWIR bands (11 and 12) in the median to high percentile distribution were the most important variables, consistent with their sensitivity to vegetation/tree water content and utility in drought detection [74,86]. The SWIR band 12 is also used to calculate NBR and NDWI₁₂, and while these indices have been frequently applied for windthrow detection (e.g., [29,33,40,73]), they did not improve our predictions of canopy cover in this study. Nonetheless, our findings align with those from elsewhere that indicate that using all available S2-bands provides more accurate results than using individual indices in modelling approaches for precision agriculture, including crop type, disease, and stress (e.g., grass, water, and nitrogen) monitoring [87], or for varying vegetation cover across landscapes [88].

Direct comparison of model performance with other windthrow mapping methods is problematic, as most previous studies have been based on classification models (as opposed to regression models) or focused on the volume of fallen trees (as opposed to percentage change in canopy cover) to quantify windthrow damage [24,38]. While our study is unique, the performance of our best random forest regression model to predict canopy cover (R^2 0.69) was comparable with that of a model based on a non-linear relationship between a modified vegetation index (derived from multispectral Landsat TM5 satellite data) and percentage tree canopy cover (derived from very-high-resolution QuickBird satellite data) that was used to quantify canopy cover loss after a severe tropical cyclone in tropical eucalypt woodlands of northern Australia (R^2 0.73; [39]).

4.4. Extent and Severity of Windthrow

The scale and size of the windthrow event was unprecedented in south-eastern Australia, with nearly 40,000 ha of damaged forest area across the Wombat Forest alone. Substantial windthrow during the same storm event also occurred in the wetter mountain ash (*E. regnans*) forests of the Dandenong Ranges National Park, about 160 km east of the study area, although a comparatively smaller area (~220 ha, [89]) was affected. Previously reported recent windthrow events in Victoria have been very localized; for example, 3.5 ha in an alpine ash (*E. delegatensis*) forest in 1998 [43] and about 8 to 10 ha in dry eucalypt forest in the Grampians National Park (180 km to the west of the study area) were affected in 2004.

This study's high-resolution prediction of forest canopy cover and its change due to windthrow enabled fine-scaled delineation and continuous mapping of windthrow across the broader Wombat Forest that ranged from low to high severity and small localized patches to extensive areas. The use of canopy cover to distinguish windthrow severity aligns well with a common Australian vegetation classification system, which uses foliage projective cover, life form, and the height of the overstorey to identify structural formations [56]. A change or decrease in canopy cover greater than 30–40% would constitute a change in the structural forest formation, i.e., from Open-Forest (70% to 30%) to Woodland (30–10%), while changes > 50% constitute the conversion of forests towards non-forest formations. Two thirds of the Wombat Forest was impacted by windthrow in the June 2021 storm event, of which 27% (~10,000 ha, or 17% of the total forest area) had a moderate

to high severity decrease in canopy cover, which has clear implications for management interventions focused on tree regeneration and forest restoration [47,90].

This highlights the importance of fine-scale windthrow severity mapping in particular to inform the management of forest areas most severely affected by windthrow. These spatially explicit data can support decisions for the prioritization of management actions to minimize imminent risks to public safety. In addition, the data indicate areas in the landscape with the most likely changes in the distribution of fuels in these fire-prone landscapes. A fuel load assessment two years after the main windthrow event in the Wombat Forest detected significant increases in near-surface and coarse fuels that could increase the intensity of planned or unplanned fires [47]. Furthermore, windthrow severity mapping provides critical information to support management towards the long-term goals of forest regeneration and habitat conservation for threatened species.

4.5. Future Research

Our future research will focus on the applicability and utility of our windthrow severity mapping in other forest types in Victoria or south-eastern Australia, i.e., the wetter eucalypt (mountain ash) forest. The expansion of baseline canopy cover estimation across different forest types and their incorporation into our regression modelling framework will not only enable the quantification and mapping of windthrow severity at landscape scales. This and our future research on automatization of plot-scale canopy cover estimation will ultimately improve and advance our windthrow severity modelling towards a more rapid detection method. Our windthrow severity modelling framework provides the opportunity to further investigate and better understand which parts of the landscape or forest structure were most susceptible to windthrow and what factors, e.g., soil moisture, topography, or management history, influenced the detected windthrow pattern. There is a strong likelihood that south-eastern Australia will experience more destructive storm events in the future, with indications that climate change will lead to more frequent and intense climate extremes that include heavy rainfall typically caused by cyclone, front, and thunderstorm occurrences [15,91–93]. Together with the frequency and intensity of severe winds, the risk of windthrow is expected to increase with changes in precipitation and associated changes to tree soil anchorage and growth [10]. This might necessitate the development of a windthrow risk framework for which our wind severity modelling framework can provide the foundation.

5. Conclusions

Our study outlines a novel remote sensing method with random forest regression modelling to delineate, map, and quantify windthrow severity as change in canopy cover across a large area in a temperate eucalypt (broadleaf evergreen) forest in south-eastern Australia. The fine-scale and continuous mapping of windthrow severity allows us to identify windthrow from low to high severity and from localized to extensive forest areas. This facilitates and informs forest managers concerning their immediate action plans to reduce future fire risk and long-term management efforts to rehabilitate damaged forest areas. With the opportunity to expand and automate our wind severity modelling framework, a more rapid mapping of windthrow severity for first response management will be possible, as well as the development for any future windthrow risk framework.

Author Contributions: Conceptualization, N.H.-N., P.D.B., S.H., A.C.B., J.E.B., T.A.F., S.J., J.C.N.U., and L.T.B.; Data curation, N.H.-N. and P.D.B.; Formal analysis, N.H.-N., P.D.B. and S.H.; Investigation, N.H.-N., P.D.B., S.H., A.C.B., J.E.B., T.A.F., S.J., J.C.N.U. and L.T.B.; Methodology, N.H.-N., P.D.B., S.H., A.C.B., J.E.B., T.A.F., S.J., J.C.N.U. and L.T.B.; Project administration, N.H.-N.; Resources, P.D.B. and S.H.; Supervision, L.T.B.; Visualization, N.H.-N. and P.D.B.; Writing—original draft, N.H.-N.; Writing—review and editing, N.H.-N., P.D.B., S.H., A.C.B., J.E.B., T.A.F., S.J., J.C.N.U. and L.T.B. All authors have read and agreed to the published version of the manuscript.

Funding: N.H.N. was funded from the Melbourne Research Fellow–Career Interruption Fellowship 2022. A.C.B was supported by an Australian Government Research Training Program.

Data Availability Statement: Dataset available on request from the authors.

Acknowledgments: The authors acknowledge the Dja Dja Wurrung, Wadawurrung, and Wurrundjeri Woi Wurrung and people as the Traditional Owners of the land on which this study was undertaken, and pay our respects to their Elders, past and present. Data layers of public land types (including forest type and water bodies), fire, and harvest history were obtained from the Victorian Department of Energy, Environment, and Climate Action (DEECA).

Conflicts of Interest: The authors declare no conflicts of interest.

References

- Allen, M.S.; Thapa, V.; Arévalo, J.R.; Palmer, M.W. Windstorm Damage and Forest Recovery: Accelerated Succession, Stand Structure, and Spatial Pattern over 25 Years in Two Minnesota Forests. *Plant Ecol.* **2012**, *213*, 1833–1842. [[CrossRef](#)]
- Everham, E.M.; Brokaw, N.V.L. Forest Damage and Recovery from Catastrophic Wind. *Bot. Rev.* **1996**, *62*, 113–185. [[CrossRef](#)]
- Mitchell, S.J. Wind as a Natural Disturbance Agent in Forests: A Synthesis. *For. Int. J. For. Res.* **2013**, *86*, 147–157. [[CrossRef](#)]
- Ulanova, N.G. The Effects of Windthrow on Forests at Different Spatial Scales: A Review. *For. Ecol. Manag.* **2000**, *135*, 155–167. [[CrossRef](#)]
- Gardiner, B.; Schuck, A.R.T.; Schelhaas, M.-J.; Orazio, C.; Blennow, K.; Nicoll, B. *Living with Storm Damage to Forests*; European Forest Institute Joensuu: Joensuu, Finland, 2013; Volume 3, ISBN 952-5980-08-1.
- FAO. *Climate Change Guidelines for Forest Managers*; Food and Agriculture Organization of the United Nations: Rome, Italy, 2013.
- Forzieri, G.; Girardello, M.; Ceccherini, G.; Spinoni, J.; Feyen, L.; Hartmann, H.; Beck, P.S.A.; Camps-Valls, G.; Chirici, G.; Mauri, A.; et al. Emergent Vulnerability to Climate-Driven Disturbances in European Forests. *Nat. Commun.* **2021**, *12*, 1081. [[CrossRef](#)]
- Pugh, T.A.M.; Lindeskog, M.; Smith, B.; Poulter, B.; Arneth, A.; Haverd, V.; Calle, L. Role of Forest Regrowth in Global Carbon Sink Dynamics. *Proc. Natl. Acad. Sci. USA* **2019**, *116*, 4382–4387. [[CrossRef](#)]
- Reichstein, M.; Bahn, M.; Ciais, P.; Frank, D.; Mahecha, M.D.; Seneviratne, S.I.; Zscheischler, J.; Beer, C.; Buchmann, N.; Frank, D.C.; et al. Climate Extremes and the Carbon Cycle. *Nature* **2013**, *500*, 287–295. [[CrossRef](#)]
- Seidl, R.; Thom, D.; Kautz, M.; Martin-Benito, D.; Peltoniemi, M.; Vacchiano, G.; Wild, J.; Ascoli, D.; Petr, M.; Honkaniemi, J.; et al. Forest Disturbances under Climate Change. *Nat. Clim. Chang.* **2017**, *7*, 395–402. [[CrossRef](#)]
- Gardiner, B. Wind Damage to Forests and Trees: A Review with an Emphasis on Planted and Managed Forests. *J. For. Res.* **2021**, *26*, 248–266. [[CrossRef](#)]
- Keenan, R.J. Climate Change Impacts and Adaptation in Forest Management: A Review. *Ann. For. Sci.* **2015**, *72*, 145–167. [[CrossRef](#)]
- Seidl, R.; Turner, M.G. Post-Disturbance Reorganization of Forest Ecosystems in a Changing World. *Proc. Natl. Acad. Sci. USA* **2022**, *119*, e2202190119. [[CrossRef](#)] [[PubMed](#)]
- Allen, J.T.; Allen, E.R. A Review of Severe Thunderstorms in Australia. *Atmos. Res.* **2016**, *178–179*, 347–366. [[CrossRef](#)]
- Callaghan, J. Analysis of the June 2021 Winter Storm in Victoria with a Catastrophic Loss of Large Trees and Major Flooding. *J. Aquac. Mar. Biol.* **2023**, *12*, 54–70. [[CrossRef](#)]
- Everham, E.M. A Comparison of Methods for Quantifying Catastrophic Wind Damage to Forests. In *Wind and Trees*; Cambridge University Press: Cambridge, UK, 1995; pp. 340–357.
- Webb, S.L. Disturbance by Wind in Temperate-Zone Forests. In *Ecosystems of Disturbed Ground*; Elsevier: Amsterdam, The Netherlands, 1999; pp. 187–263. ISBN 0-444-82420-0.
- Gardiner, B.; Berry, P.; Moulia, B. Review: Wind Impacts on Plant Growth, Mechanics and Damage. *Plant Sci.* **2016**, *245*, 94–118. [[CrossRef](#)] [[PubMed](#)]
- Rich, R.L.; Frelich, L.; Reich, P.B.; Bauer, M.E. Detecting Wind Disturbance Severity and Canopy Heterogeneity in Boreal Forest by Coupling High-Spatial Resolution Satellite Imagery and Field Data. *Remote Sens. Environ.* **2010**, *114*, 299–308. [[CrossRef](#)]
- Hu, T.; Smith, R.B. The Impact of Hurricane Maria on the Vegetation of Dominica and Puerto Rico Using Multispectral Remote Sensing. *Remote Sens.* **2018**, *10*, 827. [[CrossRef](#)]
- Kumar, R.; Rani, S.; Maharana, P. Assessing the Impacts of Amphan Cyclone over West Bengal, India: A Multi-Sensor Approach. *Environ. Monit. Assess.* **2021**, *193*, 283. [[CrossRef](#)]
- Deigele, W.; Brandmeier, M.; Straub, C. A Hierarchical Deep-Learning Approach for Rapid Windthrow Detection on PlanetScope and High-Resolution Aerial Image Data. *Remote Sens.* **2020**, *12*, 2121. [[CrossRef](#)]
- Einzmann, K.; Immitzer, M.; Böck, S.; Bauer, O.; Schmitt, A.; Atzberger, C. Windthrow Detection in European Forests with Very High-Resolution Optical Data. *Forests* **2017**, *8*, 21. [[CrossRef](#)]
- Chirici, G.; Bottalico, F.; Giannetti, F.; Del Perugia, B.; Travaglini, D.; Nocentini, S.; Kutchartt, E.; Marchi, E.; Foderi, C.; Fioravanti, M.; et al. Assessing Forest Windthrow Damage Using Single-Date, Post-Event Airborne Laser Scanning Data. *For. Int. J. For. Res.* **2018**, *91*, 27–37. [[CrossRef](#)]

25. Nyström, M.; Holmgren, J.; Fransson, J.E.S.; Olsson, H. Detection of Windthrown Trees Using Airborne Laser Scanning. *Int. J. Appl. Earth Obs. Geoinf.* **2014**, *30*, 21–29. [[CrossRef](#)]
26. Schwarz, M.; Steinmeier, C.; Holecz, F.; Stebler, O.; Wagner, H. Detection of Windthrow in Mountainous Regions with Different Remote Sensing Data and Classification Methods. *Scand. J. For. Res.* **2003**, *18*, 525–536. [[CrossRef](#)]
27. Tanase, M.A.; Aponte, C.; Mermoz, S.; Bouvet, A.; Le Toan, T.; Heurich, M. Detection of Windthrows and Insect Outbreaks by L-Band SAR: A Case Study in the Bavarian Forest National Park. *Remote Sens. Environ.* **2018**, *209*, 700–711. [[CrossRef](#)]
28. Rüetschi, M.; Small, D.; Waser, L.T. Rapid Detection of Windthrows Using Sentinel-1 C-Band SAR Data. *Remote Sens.* **2019**, *11*, 115. [[CrossRef](#)]
29. Vaglio Laurin, G.; Francini, S.; Luti, T.; Chirici, G.; Pirotti, F.; Papale, D. Satellite Open Data to Monitor Forest Damage Caused by Extreme Climate-Induced Events: A Case Study of the Vaia Storm in Northern Italy. *For. Int. J. For. Res.* **2021**, *94*, 407–416. [[CrossRef](#)]
30. Wang, F.; Xu, Y.J. Comparison of Remote Sensing Change Detection Techniques for Assessing Hurricane Damage to Forests. *Environ. Monit. Assess.* **2010**, *162*, 311–326. [[CrossRef](#)]
31. Hamdi, Z.M.; Brandmeier, M.; Straub, C. Forest Damage Assessment Using Deep Learning on High Resolution Remote Sensing Data. *Remote Sens.* **2019**, *11*, 1976. [[CrossRef](#)]
32. Kislov, D.E.; Korznikov, K.A. Automatic Windthrow Detection Using Very-High-Resolution Satellite Imagery and Deep Learning. *Remote Sens.* **2020**, *12*, 1145. [[CrossRef](#)]
33. Giannetti, F.; Pecchi, M.; Travaglini, D.; Francini, S.; D’Amico, G.; Vangi, E.; Cocozza, C.; Chirici, G. Estimating VAIA Windstorm Damaged Forest Area in Italy Using Time Series Sentinel-2 Imagery and Continuous Change Detection Algorithms. *Forests* **2021**, *12*, 680. [[CrossRef](#)]
34. Dalponte, M.; Marzini, S.; Solano-Correa, Y.T.; Tonon, G.; Vescovo, L.; Gianelle, D. Mapping Forest Windthrows Using High Spatial Resolution Multispectral Satellite Images. *Int. J. Appl. Earth Obs. Geoinf.* **2020**, *93*, 102206. [[CrossRef](#)]
35. Dalponte, M.; Solano-Correa, Y.T.; Marinelli, D.; Liu, S.; Yokoya, N.; Gianelle, D. Detection of Forest Windthrows with Bitemporal COSMO-SkyMed and Sentinel-1 SAR Data. *Remote Sens. Environ.* **2023**, *297*, 113787. [[CrossRef](#)]
36. Forzieri, G.; Pecchi, M.; Girardello, M.; Mauri, A.; Klaus, M.; Nikolov, C.; Rüetschi, M.; Gardiner, B.; Tomaščík, J.; Small, D.; et al. A Spatially Explicit Database of Wind Disturbances in European Forests over the Period 2000–2018. *Earth Syst. Sci. Data* **2020**, *12*, 257–276. [[CrossRef](#)]
37. McCarthy, M.J.; Jessen, B.; Barry, M.J.; Figueroa, M.; McIntosh, J.; Murray, T.; Schmid, J.; Muller-Karger, F.E. Mapping Hurricane Damage: A Comparative Analysis of Satellite Monitoring Methods. *Int. J. Appl. Earth Obs. Geoinf.* **2020**, *91*, 102134. [[CrossRef](#)]
38. Ritter, T.; Gollob, C.; Kraßnitzer, R.; Stampfer, K.; Nothdurft, A. A Robust Method for Detecting Wind-Fallen Stems from Aerial RGB Images Using a Line Segment Detection Algorithm. *Forests* **2022**, *13*, 90. [[CrossRef](#)]
39. Staben, G.W.; Evans, K.G. Estimates of Tree Canopy Loss as a Result of Cyclone Monica, in the Magela Creek Catchment Northern Australia. *Austral Ecol.* **2008**, *33*, 562–569. [[CrossRef](#)]
40. Olmo, V.; Tordoni, E.; Petruzzellis, F.; Bacaro, G.; Altobelli, A. Use of Sentinel-2 Satellite Data for Windthrows Monitoring and Delimiting: The Case of “Vaia” Storm in Friuli Venezia Giulia Region (North-Eastern Italy). *Remote Sens.* **2021**, *13*, 1530. [[CrossRef](#)]
41. Hateley, R.F. *The Victorian Bush: Its “Original and Natural” Condition*, 1st ed.; Polybractea Press: South Melbourne, VC, Australia, 2010; ISBN 978-0-9775240-7-5.
42. Florentine, S.; Milberg, P.; Gibson, M.; Westbrooke, M. Post-Wildfire Seedling Colonisation Patterns in a Eucalyptus Delegatensis (Myrtaceae) Windthrow Site at Snowy River National Park, Victoria. *Aust. For.* **2008**, *71*, 48–53. [[CrossRef](#)]
43. Florentine, S.; Westbrooke, M. Effects of Windthrow on a Stand of *Eucalyptus delegatensis* (Myrtaceae) and Early Understorey Succession at Snowy River National Park, Victoria. *Aust. For.* **2004**, *67*, 6206. [[CrossRef](#)]
44. Wood, M.J.; Scott, R.; Volker, P.W.; Mannes, D.J. Windthrow in Tasmania, Australia: Monitoring, Prediction And Management. *For. Int. J. For. Res.* **2008**, *81*, 415–427. [[CrossRef](#)]
45. Cremer, K.W.; Myers, B.J.; Van Der Duys, F.; Craig, I.E. Silvicultural Lessons from the 1974 Windthrow in Radiata Pine Plantations near Canberra. *Aust. For.* **1977**, *40*, 274–292. [[CrossRef](#)]
46. Turton, S.M. Landscape-Scale Impacts of Cyclone Larry on the Forests of Northeast Australia, Including Comparisons with Previous Cyclones Impacting the Region between 1858 and 2006. *Austral Ecol.* **2008**, *33*, 409–416. [[CrossRef](#)]
47. Fairman, T.A.; Symon, C.; Cawson, J.; Penman, T.D. Throwing Fuel on the Fire? Contrasting Fine and Coarse Fuel Responses to Windthrow in Temperate Eucalypt Forests in South-Eastern Australia. *For. Ecol. Manag.* **2024**, *572*, 122266. [[CrossRef](#)]
48. Collins, L.; McCarthy, G.; Mellor, A.; Newell, G.; Smith, L. Training Data Requirements for Fire Severity Mapping Using Landsat Imagery and Random Forest. *Remote Sens. Environ.* **2020**, *245*, 111839. [[CrossRef](#)]
49. Collins, L.; Griffioen, P.; Newell, G.; Mellor, A. The Utility of Random Forests for Wildfire Severity Mapping. *Remote Sens. Environ.* **2018**, *216*, 374–384. [[CrossRef](#)]
50. Tran, B.; Tanase, M.; Bennett, L.; Aponte, C. Evaluation of Spectral Indices for Assessing Fire Severity in Australian Temperate Forests. *Remote Sens.* **2018**, *10*, 1680. [[CrossRef](#)]
51. ASRIS ASRIS—Australian Soil Resource Information System. Available online: http://www.asris.csiro.au/themes/Atlas.html#Atlas_Downloads (accessed on 17 June 2019).
52. Hinko-Najera, N.; Isaac, P.; Beringer, J.; van Gorsel, E.; Ewenz, C.; McHugh, I.; Exbrayat, J.-F.; Livesley, S.J.; Arndt, S.K. Net Ecosystem Carbon Exchange of a Dry Temperate Eucalypt Forest. *Biogeosciences* **2017**, *14*, 3781–3800. [[CrossRef](#)]

53. Tolhurst, K.; Flinn, D. *Ecological Impacts of Fuel Reduction Burning in Dry Sclerophyll Forest: First Progress Report, Forest Research Report No.349*; Forest Research Centre: Sippy Downs, QLD, Australia, 1992; p. 384.
54. Bennett, L.T.; Aponte, C.; Baker, T.G.; Tolhurst, K.G. Evaluating Long-Term Effects of Prescribed Fire Regimes on Carbon Stocks in a Temperate Eucalypt Forest. *For. Ecol. Manag.* **2014**, *328*, 219–228. [[CrossRef](#)]
55. Bennett, L.T.; Aponte, C.; Tolhurst, K.G.; Löw, M.; Baker, T.G. Decreases in Standing Tree-Based Carbon Stocks Associated with Repeated Prescribed Fires in a Temperate Mixed-Species Eucalypt Forest. *For. Ecol. Manag.* **2013**, *306*, 243–255. [[CrossRef](#)]
56. Specht, R.L. Foliage Projective Cover and Standing Biomass. In *Vegetation Classification in Australia*; Gillson, A.N., Anderson, D.J., Eds.; CSIRO: Canberra, Australia, 1981; pp. 10–21.
57. Kaye, W.J. *Estimation of Tree Above-Ground Biomass across Native Forests of Victoria*; MForSc, The University of Melbourne: Parkville, Australia, 2008.
58. Tolhurst, K.G.; Victoria; Fire Management. *Effects of Repeated Low-Intensity Fire on the Understorey of a Mixed Eucalypt Foothill Forest in South-Eastern Australia*; Fire Management Research Reports; Fire Management, Department of Sustainability and Environment: East Melbourne, Victoria, Australia, 2003.
59. VAHC Victoria's Registered Aboriginal Parties. Available online: <https://www.aboriginalheritagecouncil.vic.gov.au/victoria-registered-aboriginal-parties> (accessed on 21 October 2024).
60. Poynter, M. Collaborative Forest Management in Victoria's Wombat State Forest—Will It Serve the Interests of the Wider Community? *Aust. For.* **2005**, *68*, 192–201. [[CrossRef](#)]
61. Matthews, N.; Missingham, B. Social Accountability and Community Forest Management: The Failure of Collaborative Governance in the Wombat Forest. *Dev. Pract.* **2009**, *19*, 1052–1063. [[CrossRef](#)]
62. *Nearmap Australia High Resolution Aerial Maps from the Wombat Forest Region from December 2020 and December 2021*; Nearmap: Victoria, Australia, 2022.
63. R Core Team. *R: A Language and Environment for Statistical Computing*; R Foundation for Statistical Computing: Vienna, Austria. Available online: <http://www.R-project.org/> (accessed on 21 October 2024).
64. McBain, M.; Sumner, M. Slippymath: Slippy Map Tile Tools, R Package Version 0.3.1. Available online: <https://cran.r-project.org/web/packages/slippymath/index.html> (accessed on 21 October 2024).
65. Pebesma, E. Simple Features for R: Standardized Support for Spatial Vector Data. *R J.* **2018**, *10*, 439–446. [[CrossRef](#)]
66. Olofsson, P.; Arévalo, P.; Espejo, A.B.; Green, C.; Lindquist, E.; McRoberts, R.E.; Sanz, M.J. Mitigating the Effects of Omission Errors on Area and Area Change Estimates. *Remote Sensing of Environment* **2020**, *236*, 111492. [[CrossRef](#)]
67. Pebesma, E.; Bivand, R. *Spatial Data Science: With Applications in R*; Chapman and Hall/CRC: New York, NY, USA, 2023; ISBN 978-0-429-45901-6.
68. Hijmans, R.J.; Bivand, R.; Dyba, K.; Pebesma, E.; Sumner, M.D. Terra: Spatial Data Analysis, R Package Version 1.7–78. Available online: <https://cran.r-project.org/web/packages/terra/index.html> (accessed on 21 October 2024).
69. Gorelick, N.; Hancher, M.; Dixon, M.; Ilyushchenko, S.; Thau, D.; Moore, R. Google Earth Engine: Planetary-Scale Geospatial Analysis for Everyone. *Remote Sens. Environ.* **2017**, *202*, 18–27. [[CrossRef](#)]
70. Drusch, M.; Del Bello, U.; Carlier, S.; Colin, O.; Fernandez, V.; Gascon, F.; Hoersch, B.; Isola, C.; Laberinti, P.; Martimort, P.; et al. Sentinel-2: ESA's Optical High-Resolution Mission for GMES Operational Services. *Remote Sens. Environ.* **2012**, *120*, 25–36. [[CrossRef](#)]
71. Main-Knorn, M.; Pflug, B.; Louis, J.; Debaecker, V.; Müller-Wilm, U.; Gascon, F. Sen2Cor for Sentinel-2. In *Proceedings of the Image and Signal Processing for Remote Sensing XXIII, Warsaw, Poland, 11–13 September 2017*; Bruzzone, L., Bovolo, F., Benediktsson, J.A., Eds.; SPIE: Warsaw, Poland, 4 October, 2017; p. 3.
72. *ESA Sentinel-2 Products Specification Document (PSD)*; Version 15.0; European Space Agency: Paris, France, 2024.
73. Candotti, A.; De Giglio, M.; Dubbini, M.; Tomelleri, E. A Sentinel-2 Based Multi-Temporal Monitoring Framework for Wind and Bark Beetle Detection and Damage Mapping. *Remote Sens.* **2022**, *14*, 6105. [[CrossRef](#)]
74. Marusig, D.; Petruzzellis, F.; Tomasella, M.; Napolitano, R.; Altobelli, A.; Nardini, A. Correlation of Field-Measured and Remotely Sensed Plant Water Status as a Tool to Monitor the Risk of Drought-Induced Forest Decline. *Forests* **2020**, *11*, 77. [[CrossRef](#)]
75. Kacic, P.; Thonfeld, F.; Gessner, U.; Kuenzer, C. Forest Structure Characterization in Germany: Novel Products and Analysis Based on GEDI, Sentinel-1 and Sentinel-2 Data. *Remote Sens.* **2023**, *15*, 1969. [[CrossRef](#)]
76. Gao, B. NDWI—A Normalized Difference Water Index for Remote Sensing of Vegetation Liquid Water from Space. *Remote Sens. Environ.* **1996**, *58*, 257–266. [[CrossRef](#)]
77. Kuhn, M.; Wickham, H. Tidymodels: A Collection of Packages for Modeling and Machine Learning Using Tidyverse Principles. 2020. Available online: <https://www.tidymodels.org> (accessed on 9 January 2023).
78. Breiman, L. Random Forests. *Mach. Learn.* **2001**, *45*, 5–32. [[CrossRef](#)]
79. Liaw, A.; Wiener, M. Classification and Regression by randomForest. *R News* **2002**, *2*, 18–22.
80. Wright, M.N.; Ziegler, A. Ranger: A Fast Implementation of Random Forests for High Dimensional Data in C++ and R. *J. Stat. Softw.* **2017**, *077*. [[CrossRef](#)]
81. Therneau, T.; Atkinson, B. Rpart: Recursive Partitioning and Regression Trees, R Package Version 4.1.23. Available online: <https://cran.r-project.org/web/packages/rpart> (accessed on 21 October 2024).
82. Breiman, L.; Friedman, J.; Olshen, R.A.; Stone, C.J. *Classification and Regression Trees*, 1st ed.; Chapman and Hall/CRC: Boca Raton, FL, USA, 1984; ISBN 978-1-315-13947-0. [[CrossRef](#)]

83. Kuhn, M.; Johnson, K. *Feature Engineering and Selection: A Practical Approach for Predictive Models*; Taylor & Francis: Abingdon, UK, 2019.
84. Kuhn, M.; Vaughan, D. Parsnip: A Common API to Modeling and Analysis Functions, R Package Version 1.2.1. Available online: <https://cran.r-project.org/web/packages/parsonip/index.html> (accessed on 21 October 2024).
85. Burrows, G.E. Buds, Bushfires and Resprouting in the Eucalypts. *Aust. J. Bot.* **2013**, *61*, 331–349. [[CrossRef](#)]
86. Gao, B.-C.; Goetz, A.F.H. Extraction of Dry Leaf Spectral Features from Reflectance Spectra of Green Vegetation. *Remote Sens. Environ.* **1994**, *47*, 369–374. [[CrossRef](#)]
87. Zhang, T.-X.; Su, J.-Y.; Liu, C.-J.; Chen, W.-H. Potential Bands of Sentinel-2A Satellite for Classification Problems in Precision Agriculture. *Int. J. Autom. Comput.* **2019**, *16*, 16–26. [[CrossRef](#)]
88. Lawrence, R.L.; Ripple, W.J. Comparisons among Vegetation Indices and Bandwise Regression in a Highly Disturbed, Heterogeneous Landscape: Mount St. Helens, Washington. *Remote Sens. Environ.* **1998**, *64*, 91–102. [[CrossRef](#)]
89. Victoria, F.F.M. Dandenong Ranges and Catchments. Available online: <https://www.ffm.vic.gov.au/recovery-after-an-emergency/managing-fire-risk-after-storms/dandenong-ranges-and-catchments> (accessed on 20 October 2024).
90. Fairman, T.; Hinko-Najera, N.; Bennett, L.T.; Penman, T.D. *Restoration of Storm Damaged Mixed Species Forests in Wombat and Cobaw State Forests*; FLARE Wildfire Research Group, School of Agriculture, Food and Ecosystem Science; The University of Melbourne: Melbourne, Victoria, Australia, 2023; p. 85.
91. BOM. CSIRO State of the Climate 2022: Bureau of Meteorology. Available online: <http://www.bom.gov.au/state-of-the-climate/> (accessed on 1 October 2023).
92. Dowdy, A.J.; Catto, J.L. Extreme Weather Caused by Concurrent Cyclone, Front and Thunderstorm Occurrences. *Sci. Rep.* **2017**, *7*, 40359. [[CrossRef](#)]
93. Brown, A.; Dowdy, A. Severe Convective Wind Environments and Future Projected Changes in Australia. *J. Geophys. Res. Atmos.* **2021**, *126*, e2021JD034633. [[CrossRef](#)]

Disclaimer/Publisher’s Note: The statements, opinions and data contained in all publications are solely those of the individual author(s) and contributor(s) and not of MDPI and/or the editor(s). MDPI and/or the editor(s) disclaim responsibility for any injury to people or property resulting from any ideas, methods, instructions or products referred to in the content.